SE9600086

CHALMERS UNIVERSITY OF TECHNOLOGY

DEPARTMENT OF REACTOR PHYSICS

ISSN 0281-9775

CTH-RF-114 April 1995

Scintillating Fibre Tracking Neutron Detector

by

Joakim Karlsson

Department of Reactor Physics
Chalmers University of Technology
S - 412 96 Göteborg, Sweden
ISSN 0281-9775

VOL 27 № 12

Scintillating Fibre Tracking Neutron Detector

Diploma Thesis

by

Joakim Karlsson

Supervisor: Dr. Thomas Elevant

Examiner: Prof. Imre Pázsit

Abstract

A detector for measurements of collimated fluxes of neutrons in the energy range 2-20 MeV is proposed. It utilizes (n,p) elastic scattering in scintillating optical fibres placed in successive orthogonal layers perpendicular to the neutron flux. A test module has been designed, constructed and tested with respect to separation of neutron and gamma events. The pulse height measurements show the feasibility to discriminate between neutron, gamma and background events. Application to measurements of fusion neutrons is considered.

Table of contents

1. Introduction

Neutron production rate measurements are an important tool of diagnostics of fusion plasmas. Measurements of time and space resolved neutron rates give information about the fusion rates over the plasma cross-section, from which the total fusion yield and the nuclear power production can be derived.

Neutrons born in a fusion plasma have their energy peaked around 2.45 MeV for deuterium-deuterium (DD) plasmas and 14.1 MeV for deuterium-tritium (DT) plasmas. A significant fraction of the neutrons undergo elastic and inelastic scattering, reducing their energies. These neutrons cause an undesired background in the detector.

Organic scintillators are often used for fast neutron detection and measurements. They are also sensitive to gamma radiation, which can corrupt the neutron measurement. For small scintillators this is solved using pulse amplitude discrimination. However, for the scintillator to be efficient it needs to be large. For some scintillator materials the difference in shape of the response to protons and electrons can be used for rejection of background gamma events, by means of pulse shape analysis. The long pulses needed in this case lead to limitations in the maximum count-rate.

The proposed scintillating fibre detector is intended for fast separation of high and low energy neutrons, while rejecting gamma induced events using pulse amplitude discrimination. The first tests of a fibre detector module and the first experiences drawn are presented here.

Some underlying theory of organic scintillating materials and fibres are presented in section 2. The experimental set-up is described in section 3. Section 4 contains the experiments and the results obtained, which are discussed in section 5.

2. Theory

Nuclear radiation causes some materials to scintillate in response to induced ionization. Some organic molecules have certain symmetry properties, which give rise to a π-electron structure. Transitions in the electronic energy level structure of these molecules are responsible for their scintillating properties. This is in contrast to crystalline inorganic scintillators, e.g. CsI and NaI, which depend on the energy states determined by the crystal lattice. Since the scintillating properties of organics arise within the molecules, they scintillate independent of their physical state. Therefore, organic scintillators can appear either as a solid, as a liquid, as a vapor or as part of a multicomponent solution.
The use of scintillators is one of the most established techniques for radiation detection and continuous developments and improvements have kept them in common use for many years.

One line of development is the scintillating fibre, which has been used for making track image detectors [1,2], calorimeters [3,4] and vertex detectors [5,6]. Greatest interest in the use of scintillating fibres has been shown in the field of high energy physics research. Only a few attempts have been made to use fibres for the detection of neutrons. A good example is Yariv et al. [7], who proposed a stack of square plastic scintillating fibres for use as a fast neutron detector, able to reject strong background of γ and low energy neutrons.

Basic texts treating conventional organic scintillators can be found in Refs. [8,9,10] and some articles on scintillating fibres in Refs. [1,11,12].

2.1 Light yield and the scintillation mechanism

The scintillation efficiency is defined as the fraction of the incident energy converted into fluorescent light. The plastic scintillator is often made of an organic scintillator dissolved in a solvent, which is polymerized to give a solid solution. For example, an organic scintillator is dissolved in a styrene monomer, which is polymerized to form polystyrene plastic. The scintillation process in a plastic scintillator involves the loss of energy from the incident radiation to the solvent. The energy is then transferred to the molecules of the organic scintillator, which get excited and deexcite emitting prompt fluorescence light. The light emission falls exponentially with a decay constant depending on the life time of the excited state. There are also processes which include the emission of weak phosphorescence and delayed fluorescence light. Other deexcitation mechanisms convert the energy into heat, i.e. lattice vibrations.

A simple exponential model of a scintillation event in a fast plastic scintillator is shown in Fig. 1 [10]. This model shows the typical time behaviour consisting of a fast rise time, about 0.5 ns, and a slower decay constant, 1-4 ns, for the prompt fluorescence light.

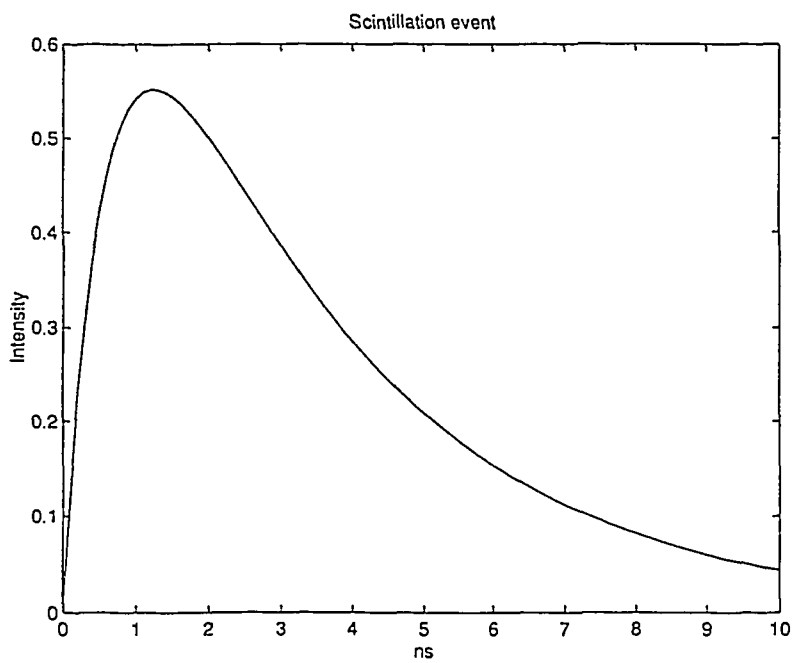

Fig. 1. Time trace of the emitted intensity from a scintillation event.

Charged particles incident on an organic scintillator lose their energy by electromagnetic interactions with the electrons. To be detectable, neutrons and γ need some reactions to transfer their energy to a charged particle, which can cause scintillation. The low atomic number of the organic scintillator constituent atoms makes Compton scattering the dominant mode of interaction, which gives a recoil electron and a scattered γ. The electron can emerge with energies ranging from zero to a maximum energy, the so called Compton edge. The exact shape of the continuum is described by the Klein-Nishina cross section, and it depends on the energy of the incident γ. The general shape of the electron energy distribution is shown in Fig. 2. A review of Compton scattering can be found in Ref. [10].

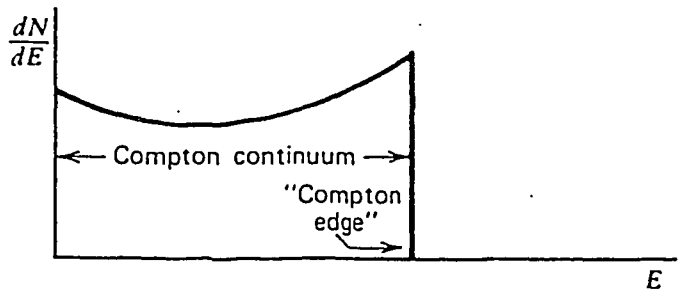

Fig. 2. The general shape of the Compton electron energy distribution [10].

For neutrons with energies 0.02-15 MeV, the most probable types of interactions are elastic scattering with hydrogen and carbon, inelastic scattering with carbon and the reactions $^{12}C(n,n')C^{*} \rightarrow 3\alpha$ and $^{12}C(n,\alpha)^{9}Be$. If the neutron energy exceeds about 5 MeV, a number of different inelastic reactions can occur with carbon. The recoil nucleus will be left in an excited state, emitting γ-radiation as it deexcites. At lower energies the main reaction is elastic neutron scattering with hydrogen and carbon. The recoil particles are ionized in the scattering process and they can therefore cause scintillations as they travel from the point of interaction.

The (n,p) elastic scattering is of particular interest for the detection of neutron events. The high hydrogen content of organic scintillators makes them well suited in this respect. The recoil protons have an approximately rectangular response function. Their energies vary between zero and the energy of the incident neutron, depending on the angle of scattering. This can be seen in Fig. 3. The governing equation is $E_p = E_n \cos^2\theta$, where θ is the angle between the incident neutron and the scattered proton. The kinematics of the neutron elastic scattering can be found in Ref. [10].

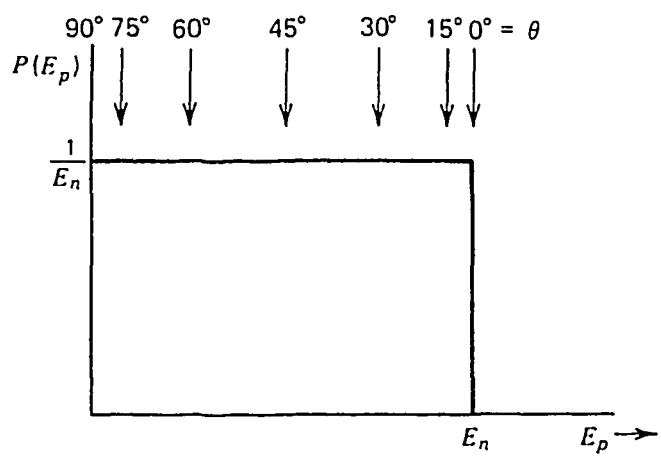

Fig. 3. Energy distribution of recoil protons produced by monoenergetic neutrons [10]. Recoil energies are indicated for various values of the recoil emission angle θ as given by $E_p = E_n \cos^2\theta$.

The light yield as a function of energy for electrons is linear for energies above about 150 keV. The response to heavier charged particles is always less than for electrons of equivalent energies. Protons give the highest light output of all heavy charged particles, and it is roughly proportional to $E^{3/2}$ for energies below 5 MeV and becomes linear for higher energies. The difference in light yield between different particles can be explained by assuming that a high ionization density along the track of the particle leads to quenching, i.e. radiationless dissipation of energy caused by the annihilation of the created charges.

The probability of annihilation limits the amount of deposited energy, that can be converted into light photons by a small volume of the scintillator. Thus high ionization density along the track leads to saturation and lowering of the scintillation efficiency.

To take into account the saturation effects of the scintillator, one expresses the light yield of heavy charged particles in the corresponding equivalent electron energy (MeVee). This relates the energy of a heavy charged particle to the energy of an electron, that generates the same amount of light in an organic scintillator. The differential energy loss (dE/dx) for an electron and a proton versus the distance from the end of the particle track is shown in Fig. 4. Also shown is the differential light output (dL/dx) for protons expressed in electron equivalent units. The difference in differential energy loss, between electrons and protons of equivalent energies, accounts for the large difference in path length as well as the difference in light yield. Indicated are also the ranges of electrons and protons for some initial energies.

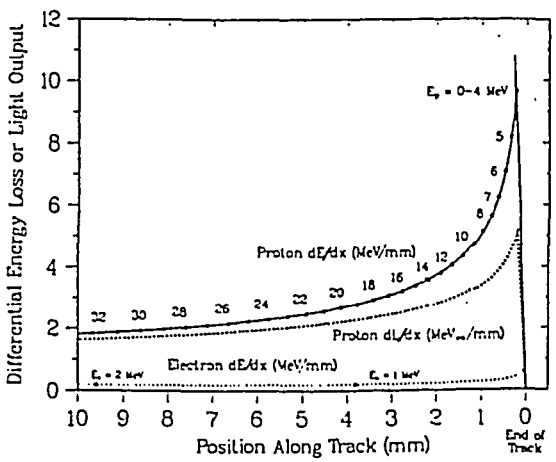

Fig. 4. The differential energy loss and light output for protons, the solid and heavy dotted curves, and electrons, the light dotted curve, versus the distance from the end of the particle track. From Ref. [7].

The equivalent electron energy as a function of proton energy for the NE102 plastic scintillator can be found in Fig. 5. A similar relation holds for the plastic scintillating fibres. There are only small differences in light output from protons for different organic scintillators.

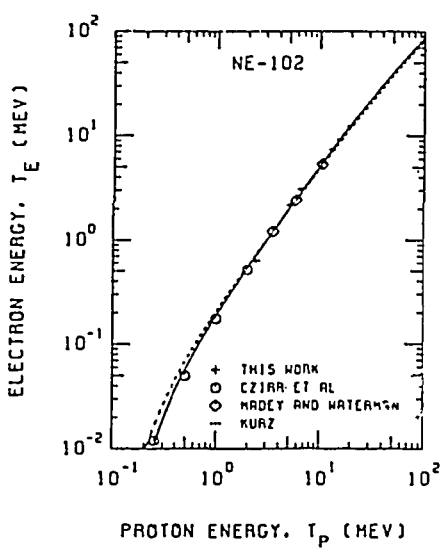

Fig. 5. Equivalent electron energy versus proton energy for NE102. From Ref. [13].

Birks [9] suggests a relation between the fluorescent energy emitted per unit path length and the specific energy loss for the particle, taking into account the possibility of quenching.

$$\frac{dL}{dx} = \frac{S\frac{dE}{dx}}{1 + kB\frac{dE}{dx}} \qquad (1)$$

The product kB is treated as an adjustable parameter to fit experimental data, and S provides the normalization of the response. Applied to electrons with small dE/dx, the following simplification holds:

$$\frac{dL}{dE} = S \qquad (2)$$

This results in the light output being linearly related to the energy of the electron and S is the normal scintillation efficiency. In the case of the BCF12 scintillating fibre, S is equal to 2.4% according to the manufacturer's specifications. Applied to heavy charged particles with large dE/dx, saturation of the light output occurs:

$$kB\frac{dE}{dx} >> 1 \Rightarrow \frac{dL}{dx} = \frac{S}{kB} \qquad (3)$$

Depending on the specific energy loss, different particles will give rise to different light yields between these two extremes.

Other models have been developed to fit experimental data more accurately. Chou [14] added one more fitting parameter in the denominator of Eq. (1), to take second order saturation effects into account. Craun and Smith [15] have made an extensive analysis of the response of a number of organic scintillators.

2.2 Techniques for the separation of neutron and γ induced events

When counting neutrons from a fusion plasma there is always a background of γ-radiation. The detectors are sensitive to γ's, as well as neutrons, which will corrupt the measurement, if no γ discrimination technique is used.

The pulse amplitude technique is the oldest and most common solution. It is based on the fact that electrons, because of their long range, will escape a small scintillator without depositing their total energy. Protons on the other hand deposit all of their energy and a small scintillator therefore gives a greater response for protons than for electrons. The signal amplitude can be used to separate γ induced electrons from recoil protons. The detection efficiency is however low for such a small scintillator, and to measure low neutron fluxes one would need large scintillator volumes, but then the γ background interferes.

2.2.1 Pulse shape discrimination

Another solution allowing the use of large scintillators, is the pulse shape discrimination technique (PSD). It is based on the fact that a long-lived component of the scintillation light, called delayed fluorescence, appears in many scintillating materials. The yield curve can often be represented by two exponential decays, one fast and one slow component. The fraction of light that appears in the slow component depends on the specific energy loss of the particle, i.e. the nature of the exciting particle. Particles with large specific energy loss will have a greater fraction of their scintillation light in the slow component, see Fig. 6. One can make use of this dependence to discriminate between particles, for example electrons and protons. The slow component typically has a decay time of several hundred nanoseconds. The PSD technique uses this long tail to distinguish between electron and proton induced scintillations. The count-rate capability will be limited by the duration of the tail.

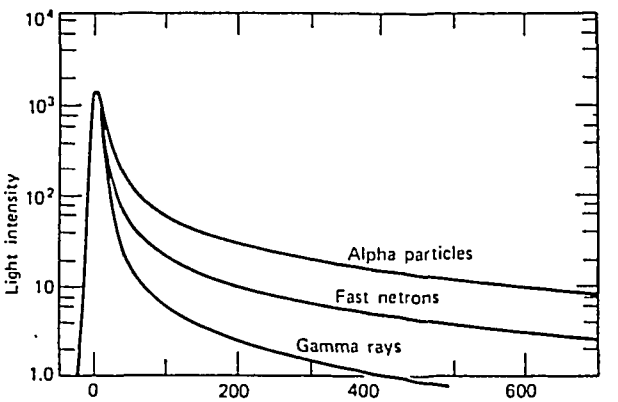

Fig. 6. Scintillation light intensity versus time [10]. This figure shows the response for particles of different nature. The differences are used in the PSD technique.

2.2.2 Discrimination for scintillating fibres

Plastic scintillators are inherently very fast, FWHM (full width of the light yield at half maximum) is often below 5 ns, i.e. the fast component. To utilize this inherent high count-rate capability, discrimination has to be performed by some other means than PSD. One answer is to use scintillating optical fibres. The fibres can be thought of as small scintillators and amplitude discrimination can be used individually on each fibre. To provide a high efficiency, the fibres can be put together forming a large volume of material. Thus it is possible to achieve both high efficiency, good γ discrimination and high count-rate with a fibre detector. The problems are the low light yield of the fibres and the complexity of the system.

2.3 Light propagation and attenuation in an optical fibre

Snell's law describes the optical refraction at an interface between two media of different refractive indices. There are several interfaces in an optical fibre: The core-cladding, cladding-air or cladding-EMA (Extra Mural Absorber).

The basic law of refraction gives the critical angle (θ_c) above which total internal reflection will occur:

$$\text{critical angle } \theta_c = \arcsin \frac{n_{clad}}{n_{core}} \tag{4}$$

where n_{core} and n_{clad} are the refraction indices of the core and cladding, respectively. Some data for BCF12 scintillating fibres are presented in Appendix 1, from where it is evident that the fibres used in this work have a critical angle of 68.6 degrees. In an optical fibre the core-cladding interface gives rise to almost perfect total internal reflections for angles larger than the critical angle. Light rays incident above the critical angle will suffer very little attenuation, while experiencing multiple reflections along the length of the fibre. This gives the "core" light a long attenuation length. The small attenuation in the core that does exist, is due to absorption in the material. If the angle is less than the critical angle partial reflection, called Fresnel reflection, will occur. The transmitted fraction will reach the next interface. Fig. 7 shows the light guiding properties of a fibre coated with white EMA.

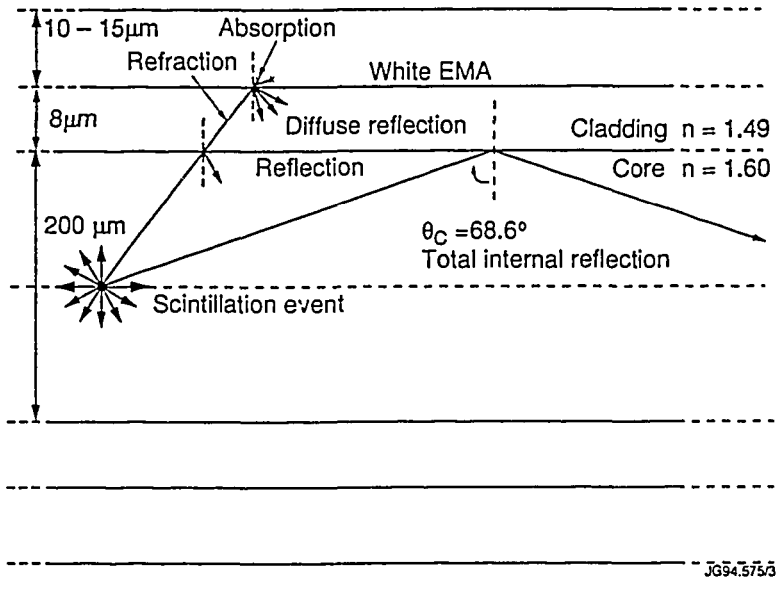

Fig. 7. The scintillating fibre as a light guide. The fibre has the characteristics of the fibres used in our tests.

The trapping efficiency, i.e. the fraction of the light trapped by internal reflections at the core-cladding interface, depends on the critical angle. The smaller the critical angle is, the more light will be trapped. The trapped fraction of light, travelling along one direction in the core of a square fibre, is calculated using the integral (5), from Ref. [1]:

$$\frac{4}{4\pi}\int_{\theta=\theta_c}^{\frac{\pi}{2}} \sin\theta \, d\theta \int_{\phi=\cos^{-1}(\cos\theta_c/\sin\theta)}^{\frac{\pi}{2}} d\phi = \frac{1}{\pi}\left[\frac{\pi}{2}\cos\theta_c - \int_{\theta_c}^{\frac{\pi}{2}} \sin\theta \cos^{-1}\left(\frac{\cos\theta_c}{\sin\theta}\right) d\theta\right] \tag{5}$$

The angles θ and ϕ are the angles describing the direction of an emitted light photon in a coordinate system with its y-axis along the direction of the fibre, see Fig. 8.

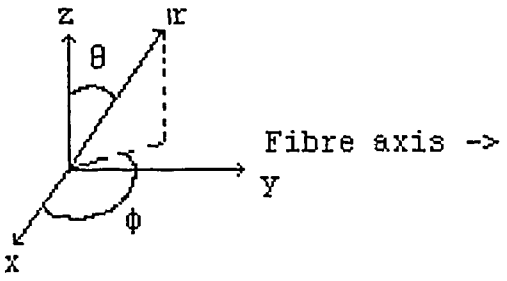

Fig. 8. The coordinate system used in the equation for the trapping efficiency of a square fibre.

The square fibres used have a trapping efficiency of 4.4% in each direction for light propagating in the core. Further, an interesting feature is that the trapped fraction of light from a scintillation event is independent of the event's location in the fibre. This is in contrast to circular fibres, where the trapping efficiency is dependent on the position of the emission within the fibre [1].

The fibres are supplied with or without EMA. Without EMA the outermost interface is the one between cladding and air. At this interface the difference between the refractive indices of the cladding and air is large, which leads to a smaller critical angle. Therefore, a larger fraction of the light will undergo total reflection at this interface than at the core-cladding interface, leading to a larger total trapping efficiency. The reflections at this interface are very much dependent on the quality of the surface of the fibre. If the surface is of very uniform quality, an appreciably large fraction will be trapped. In reality the surface quality is hard to control, and handling of the fibres quickly decreases the amount of light that is internally reflected from the cladding-air interface. The imperfections at the surface of the fibre cause the short attenuation length of the light trapped by the cladding-air interface. For further details see Ref. [12].

Light transmitted out of the fibre can cause cross-talk in adjacent fibres. To avoid this, the surface is coated with an EMA. Black EMA will absorb light at the cladding-EMA interface, and leave only the fraction of light trapped in the core. This gives a uniform light output. White EMA gives a greater light output at short distances, i.e. a few cm, because of diffuse reflections at the cladding-EMA interface. However, the light in the cladding is quickly attenuated, due to interface defects, and at longer distances, i.e. tens of cm, fibres with white EMA will yield about the same amount of light as fibres with black EMA.

The fibres used in this work are coated with white EMA on delivery. Due to poor quality of the EMA and the extensive handling of the fibres, the surfaces of the fibres have been only in part still covered at the time of use. The surfaces have also been roughened during the assembly of the experiment, and one can therefore assume that the "clad" light has a very short attenuation length. It is also possible that cross-talk could occur. If the distance from the event to the photo detector is more than a few tens of centimeters, very little of the "clad" light will remain to be recorded. On the other hand, an event very close to the photo detector would probably have a large fraction of the total light yield from the "clad" light.

2.4 Time dispersion

Light travels at different speeds in the core and cladding, due to the difference in the refractive indices. The resulting spread in arrival times of the photons at the photo detector causes time dispersion of the signal. Another factor causing time dispersion is light rays travelling along the fibre in paths with different lengths. The difference in arrival times has been calculated to be of the order of 400 ps/m fibre in both cases. For the fibre lengths used, this is much less than the duration of a scintillation event and is therefore of no consequence in this work.

3. Experimental set-up

3.1 Design of the test detector

The test detector has been designed with layers of fibres in a row in parallel and on top of each other. The layers are connected to separate photo detectors. A particle incident on the detector will penetrate some layers and cause scintillations along its track. Due to differences in differential energy loss, protons deposit their energy in a few successive layers, while electrons deposit their energy in many layers. The light output from a single layer is then large for a proton and small for an electron. Hence pulse amplitude discrimination can be used to reject γ induced events, while maintaining high efficiency, see sect. 2.2.2. This type of detector also resolves the track of the particle. Differences in path length of different particles can be exploited. In principle this can be used for separation of low and high energy protons.

The primary aim with this study is to check the feasibility of pulse height discrimination against recoil electrons. A secondary aim is to find the number of fibres fired in response to γ and neutron induced events. The fibres used are 0.2 mm square, BCF12 blue scintillating fibres partially covered by white EMA. To provide high efficiency, the detector should have as large a volume as possible with the number of fibres available. The photo detectors used are four Philips XP2020 photomultiplier tubes. The design of the test detector is limited by these constraints in equipment and the following design has been used:

The scintillating optical fibres are placed side by side in a layer. The layers are placed on top of each other in a holder. Every third layer is coupled to the same PM tube. A monitor tube is optically coupled to all remaining free ends. In a real application these ends will preferably be coated with a material of high reflectivity to achieve a larger signal amplitude at the PMT's. A schematic figure of the test detector set-up is shown in Fig. 9.

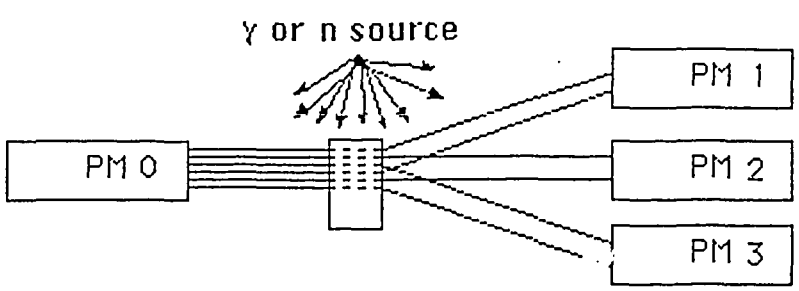

Fig. 9. The test detector set-up, showing the three PMT's on the right side and the monitor tube on the left. The three tubes are each one coupled to every third layer of the fibres.

3.1.1 Light yield

To give an estimate of the light output originating from a recoil proton one has to take several parameters into account: the dimension of the fibres, the angle and energy of the recoil proton and the position of the fibre relative to the proton track. The last parameter is due to the nonlinear behaviour of the specific energy loss for protons. The γ response, on the other hand, is almost linear and only the energy and angle of the scattered Compton electron is of interest.

The "core" light output from the first traversed fibre relative to the track of the recoil particle can be estimated if we assume the following:

The recoil particle is incident perpendicular to the fibre axis.
The attenuation of the "core" light is negligible.
Perfect optical coupling to the PMT.
The light output of the scintillating fibres is assumed to be similar to that of NE102 plastic scintillator.

The electron equivalent energy (E_{ee}) deposited in one fibre is used to estimate the fibre light output. The differential energy loss is line integrated over the width of the fibre or the total track length of the recoil particle, whichever is shortest. Empirical formulas and relations are used to obtain the E_{ee} deposited in one fibre. The number of photons (N) reaching each end of the fibre is then given by:

$$N = \frac{(E_{ee} \times S_{eff} \times T_{eff})}{E_{ph}} \qquad (6)$$

The scintillation efficiency (S_{eff}) for a minimum ionizing particle, i.e. an electron, is equal to 2.4% for the fibres used. The trapping efficiency (T_{eff}) is 4.4% as mentioned earlier. The photon energy (E_{ph}) at the wavelength of maximum emission, i.e. 435 nm, is 2.85 eV.

Table 1. Estimated number of photons emitted from one fibre end, when the fibre is penetrated by electrons and protons respectively. The resulting number of photoelectrons in a PMT with 20% quantum efficiency (QE) is also given.

Recoil energy (MeV)	Energy (MeV_{ee})	Energy deposited in first fibre (MeV_{ee})	Number of photons, N	Number of photoelectrons (20% QE)	Ref.
0.5 MeV proton	0.04	0.04	15	3	[16]
2.5 MeV --"--	0.7	0.7	248	50	[16]
14 MeV --"--	8.0	0.5	185	37	[13]
1 MeV electron	1.0	0.04	15	3	[8]
0.5 MeV --"--	0.5	0.04	15	3	[8]

The 0.5 and 2.5 MeV protons are completely stopped in one fibre, because of their short path lengths. The 14 MeV proton on the other hand will penetrate through several fibres. The value given in Table 1 is the minimum number of photons, that are emitted from the first completely penetrated fibre along the proton track. The electrons deposit their energy approximately linearly and they traverse many fibres.

The average number of photons emitted, and the corresponding number of photoelectrons, in each traversed fibre is also given. The values indicate what signals to expect from protons relative to electrons, when the fibres are used in experiments.

3.1.2 Efficiency

The efficiency of the test detector can be estimated from equation (7), Ref. [10]:

$$\varepsilon_{eff} = \frac{N_H \sigma_H}{N_H \sigma_H + N_C \sigma_C} \{ 1 - \exp[- (N_H \sigma_H + N_C \sigma_C) d] \} \qquad (7)$$

where N is the number of atoms per cm^3, σ is the microscopic scattering cross section and d is the depth of the detecting material. The detector depth is here taken to be 51 layers times 0.2 mm across each layer, which gives 1.02 cm active scintillator. The values of σ and N are taken from Ref. [10] and the manufacturer's data sheet, respectively. For 14.1 MeV neutrons, equation (7) gives $\varepsilon_{eff} = 3.4\%$ and for 2.45 MeV neutrons $\varepsilon_{eff} = 11\%$. The use of a threshold level causes some recoil protons not to be recorded by the electronics, and the efficiency decreases accordingly.

3.2 Construction of the detector

The fibres are cut into lengths of approximately 28-31 cm. They have a roughened surface and are only partially coated with EMA, see Fig. 10. The total width of the fibres is measured to 220-240 μm square.

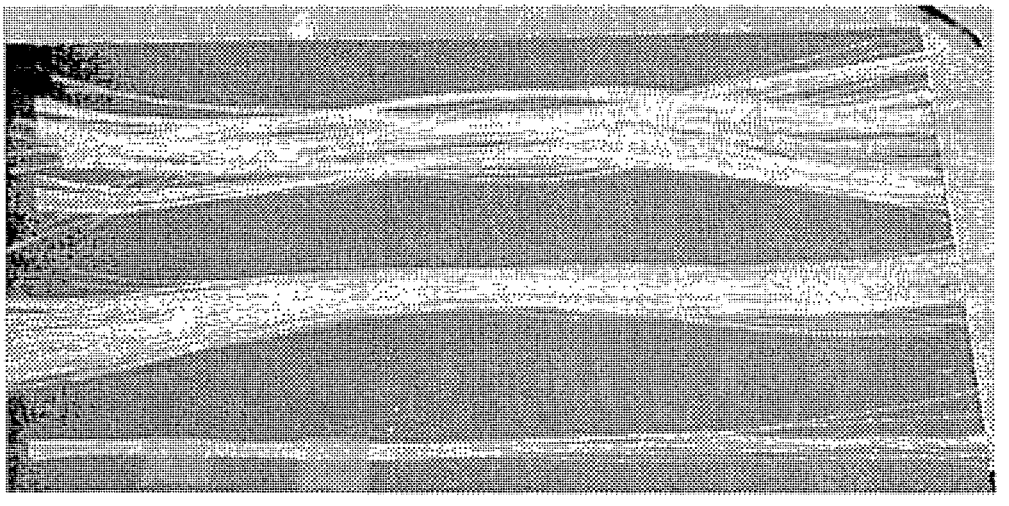

Fig. 10. At the top, the fibres before use. At the bottom, one fibre layer.

To be able to hold the fibres fixed in the desired geometry, a plastic holder has been made from two 3 mm thick, black plastic pieces. These are glued to either side of a 5 mm thick, clear plastic piece. The black pieces make up the walls and the clear piece the bottom of the holder. The fibres are placed side by side in the plastic holder, covering the 5 mm space between the holder's walls. Adhesive is then used to fasten the fibres into a layer. The layer is removed and a new layer is made. One layer consists of 18 or 19 fibres side by side.

Due to the thicknesses of the cladding and EMA, only about 3.6 mm is occupied by scintillating material of the available 5 mm space in the holder.

The layers are placed on top of each other in the holder. The 20 mm deep holder is able to contain 51 layers, which equals 10.2 mm of scintillating material. The length of the holder is 25 mm. These values give a total volume of scintillating material of 0.92 cm^3. The inner volume of the holder is 2.5 cm^3 and consequently 37% of the holder's inner volume has scintillating properties.

To fix the fibre ends to the PM tubes, four 50 mm diameter discs are cut from a 1 cm thick, black plastic board. In three of them 20 holes of 1.5 mm diameter are drilled. This diameter is selected because it is possible to fit a maximum of 20 fibres, corresponding to one layer, in the hole. The fibres of one layer is then fitted into one hole in the first of the three discs. The next fibre layer is put into the second disc, and the third fibre layer in the third disc. The fourth fibre layer is then put into the first disc. This procedure is repeated until all fibre layers are put into a hole in a disc, and it is conducted in such a way that every third layer is fitted into the same disc, see Fig. 11.

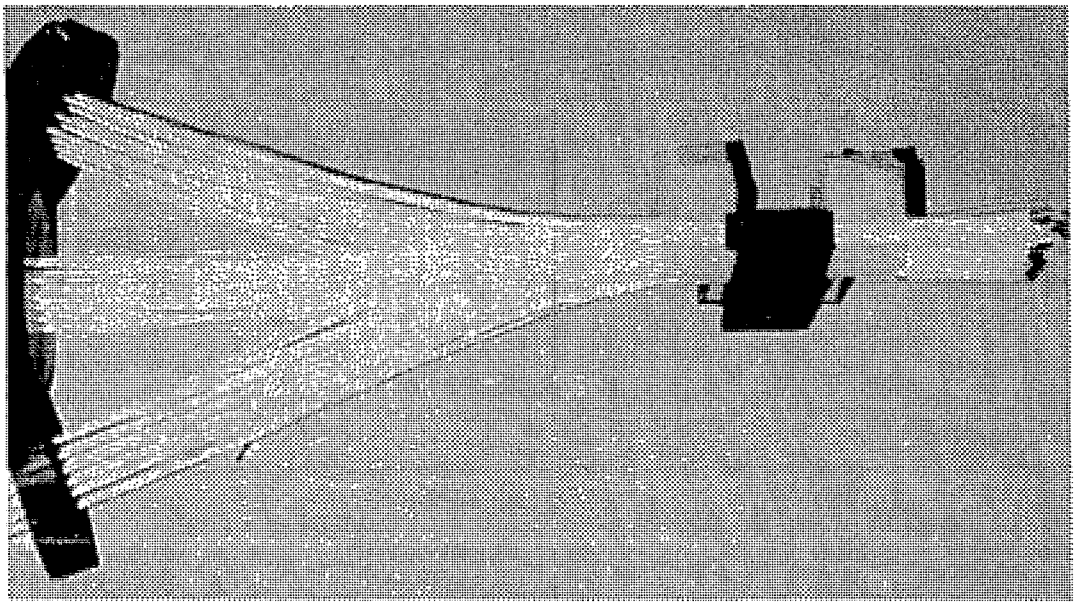

Fig. 11. The fibre layers placed in the holder with their ends put into the discs.

The disc left has been drilled with a 5 mm diameter drill making several holes close to each other. These holes interfere and create a large rectangular hole, but with the short sides shaped as half circles. The remaining free ends of the fibre layers are fitted into this hole. The layers are thereafter glued to their holes using two component epoxy. The glue used is EPO-TEK 353ND manufactured by Epoxy Technology, inc.

The fibre ends coming out of the discs are cut and polished to accomplish good optical coupling to the photo detectors. Light detection is achieved with 4 Philips XP2020 photomultiplier tubes. To achieve good optical coupling of the fibre ends to the PMT's, optical grease is used between the plastic discs and the photomultiplier tubes. After mounting μ-metal shields on the PMT's and placing the holder on a square aluminium pipe, the experimental set-up is in the state displayed in Fig. 12. The holder is approximately 4 cm from the photocathode of the monitor tube PMT0. The length of the holder is 2.5 cm.

The distance to the three PMT's from the holder is 20 cm. The total length of the fibres is then approximately 26 cm.

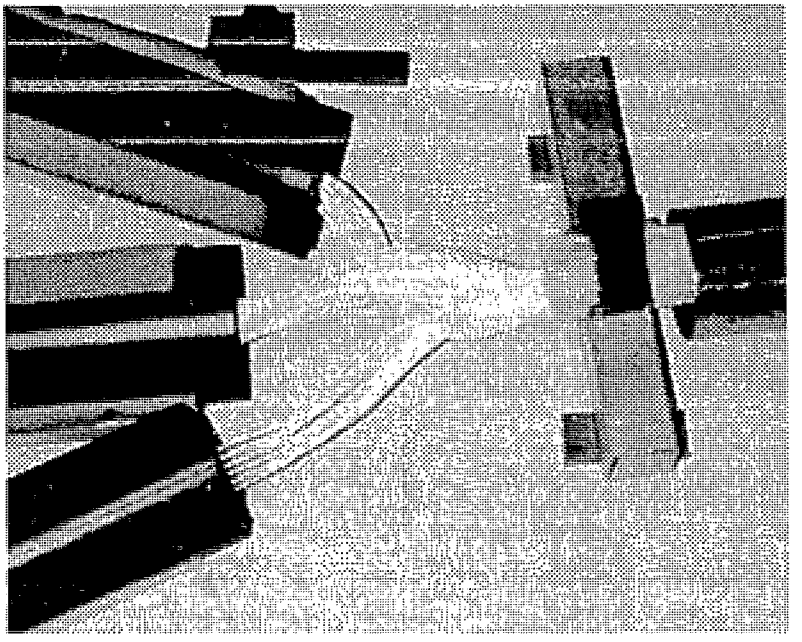

Fig. 12. The experimental set-up. Three PM tubes to the left and the monitor tube to the right.

The PMT's are connected to the signal electronics and the high voltage power supplies. There is one supply for each PM tube. Aluminium foil is used to protect the fibres and the PMT's from unwanted light. The final test device is shown in Fig. 13.

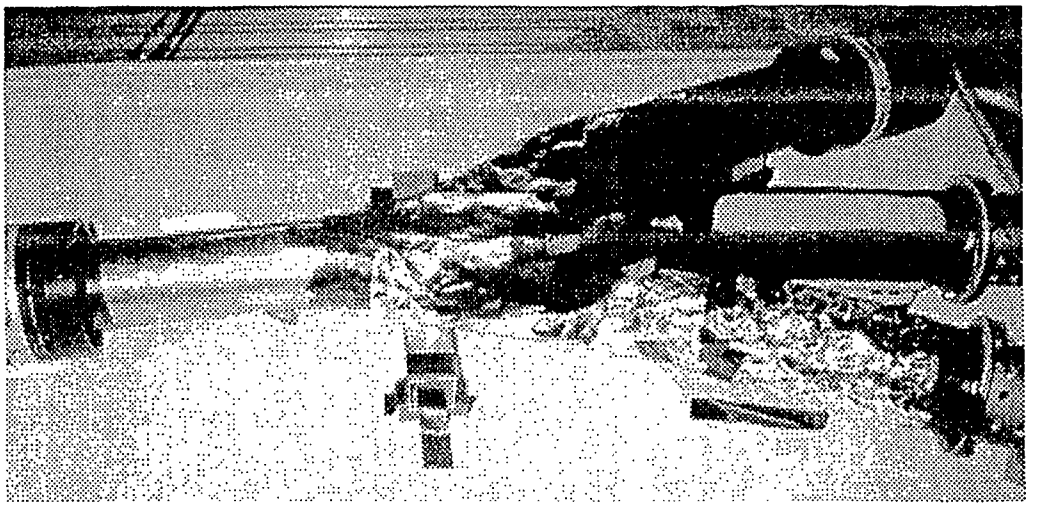

Fig. 13. The covered experimental assembly, connected and ready to use with a radiation source.

3.3 Radiation sources

The radiation sources used are: 3 Ci AmBe neutron source, 1.0 MBq ^{137}Cs (0.662 MeV) and 1.6 MBq ^{60}Co (1.17 MeV, 1.33 MeV) γ-sources. The neutrons are emitted in a wide spectrum of 1-11 MeV, with the largest fraction between 2.5 and 6 MeV. The source strength is about $7x10^5$ n/s and it also emits approximately 10^4 γ/s.

4. Experiments

In the experiments, the sources are placed a few cm in front of the holder on the square aluminium pipe. The fibres protrude from the holder towards their respective PMT's. The protruding parts of the fibres are further away from the source, but exhibit a much larger scintillating volume than the part inside the holder. No radiation shielding is used to protect the protruding part of the fibres in most of the experiments performed. The probability for an event to occur in a fibre is of the same order of magnitude for positions inside and outside the holder.

4.1 Spectra showing the number of fibres fired

To be able to study the number of fibres fired in different layers, the electronics are connected in the following manner, see Fig. 14:

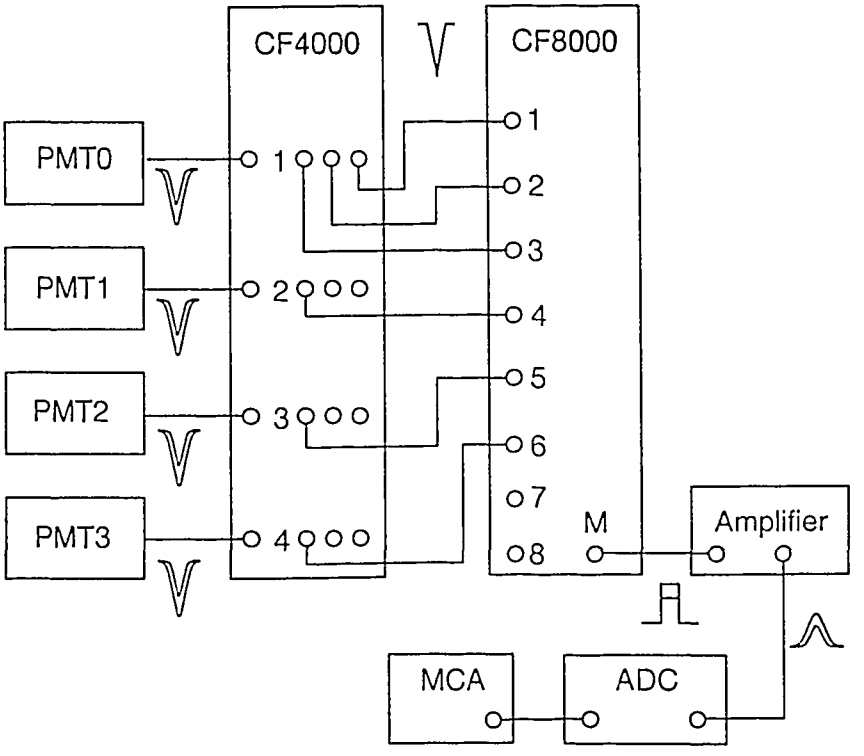

Fig. 14. The electronic set-up for spectra showing the number of fibres fired.

The signal cables from the PMT's are connected to an EG&G-ESN Quad Constant Fraction Discriminator (CF4000) with 4 channels, one for every PMT. The monitor tube, PMT0, is plugged into the first channel and PMT1, 2 and 3 to the subsequent three. For each channel on the CF4000 two standard outputs and one output with variable pulse width are provided. The width of the latter is set, giving all outputs the same standard pulse width.

When a signal with an amplitude above threshold appears at the input, a standard timing signal is provided at the output. The three outputs from channel one on CF4000 are connected to the first three inputs on an EG&G-ESN Octal Constant Fraction Discriminator (CF8000) with 8 channels. One of the outputs from each of the channels 2-4 on CF4000 is connected to the channels 4-6 on CF8000. There is a multiplicity output on CF8000, designated M, which gives a signal proportional to the number of accepted input signals. The signal from channel one on CF4000 has therefore a weight equal to three times the signal from any of the other channels at the output M on CF8000. The output M is connected to an amplifier followed by a LeCroy ADC and a multichannel analyzer(MCA). The signal fed to the MCA thus has a discrete amplitude uniquely related to the number of fibres fired.

An example of the type of spectra obtained with this setting, a low discriminator level of about 10 mV and the ^{60}Co source, is shown in Fig. 15.

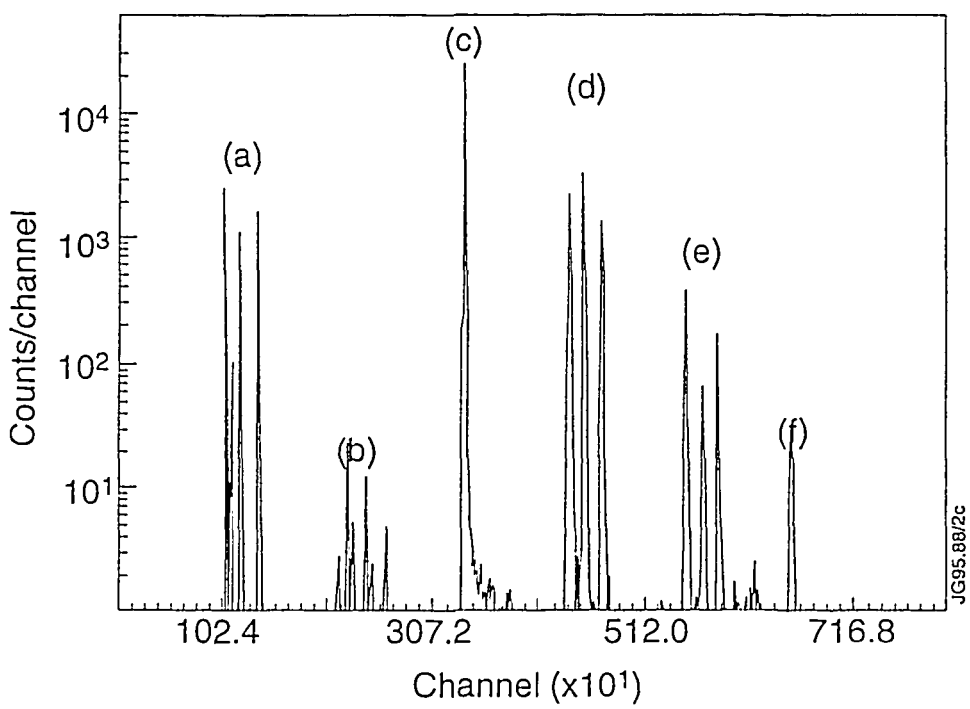

Fig. 15. Spectrum showing the number of fibres fired for a ^{60}Co γ source.

There are 6 regions in the spectrum, referred to as (a) to (f), with either one or three peaks corresponding to the amplitude of the CF8000 output M. Due to the multiplicity output M delivering signals with slightly different amplitudes, depending on which of the channels, i.e. PMT's, are included, there are three peaks in some regions. The first three peaks to the left (a) correspond to one and only one of PMT1-3 giving a signal. The simplest explanation to these counts is PM tube or electronic noise, although the major part is not. Most of the counts are due to events which emit enough light to be recorded in either of PMT1-3, but not enough light to be noticed by PMT0 on the other end of the fibre. For events occurring close to the face of either of PMT1-3, the large trapping efficiency of the "clad" light for short distances, compared to the 4% trapping efficiency of the "core" light, leads to a larger signal amplitude at PMT1-3 than at the monitor tube.

The probability that the signal exceeds the discrimination level is therefore correspondingly higher for PMT1-3 compared to PMT0. Therefore, some events will be recorded by either of PMT1-3, without the monitor tube responding.

The next region (b) also consists of three peaks. They are combinations of two accepted input signals both from PMT1-3, i.e. PMT1+PMT2, PMT1+PMT3 or PMT2+PMT3. The probability that any two of these PMT's respond simultaneously to noise is very unlikely. The probability that a particle will traverse fibres, leading to signals in two PM tubes, without the monitor tube responding, is also very small. The reason why this is at all possible is the earlier mentioned great attenuation of the "clad" light. Despite that the monitor tube sees all the fibres, it will then not react to this event. In line with the above discussion, one can assume that this region will have few counts compared to most other regions, which is the case in all our recorded spectra.

The monitor tube alone answers for the events occurring in the next region (c). This single peak has the greatest number of counts. The PMT0 tube sees all fibres, i.e. three times as many as each one of PMT1-3. The total light output is therefore divided between PMT0 on one end and the three PMT1-3 on the other. The probability of detection of an event is then greater for PMT0 than for any of PMT1-3. The problem with different light attenuation lengths for "core" and "clad" light also applies here. There are also counts due to noise from the PMT's and from the electronics. Further, highly unlikely events appearing when the three PMT1-3 give signals simultaneously, without PMT0, will also appear in this peak. These counts are fewer than the ones in the second region, and are therefore an insignificant small fraction of the counts in this peak.

The regions (d), (e) and (f) have a decreasing number of counts. The region (d) corresponds to PMT0 in combination with one and only one of the PMT1-3 giving a signal to the M output. This is similar to region (a), but with the monitor tube, PMT0, also recording the event. In the same manner the region (e) corresponds to the second region plus PMT0. The region (f) consists of a single peak, which corresponds to all four PMT's responding to an event simultaneously.

Altering the discriminator levels to 100 mV for γ induced signals from PMT1-3, causes no events to be recorded in the regions (e) and (f) and the number of counts in (d) is much less than with a 10 mV discrimination level. Thus, events that appear, using a discriminator level of 10 mV, but not with a level of 100 mV, have in general low light output, caused by the attenuation in the fibre. Events occurring in fibres close to or inside the holder show this behaviour.

The same qualitative behaviour as with a γ-source is shown in a spectrum recorded with a neutron source, see Fig. 16.

4.2 Test of the feasibility to select an energy window

When placed in a collimated neutron beam, the number of successive fibres that fire depend on the path length of the proton recoils. The path length depends on the energy and restrictive conditions imposed on the path length can therefore be used to provide a coarse energy window. For example one can choose to accept signals only when at least two successive fibres fire. This condition would certainly exclude low energy proton recoils.

Fast neutrons would only be seen if their proton recoils have high enough energies, i.e. the protons have to be scattered in a forward directed cone. The closer the neutrons are to the low energy limit, the smaller the angle of the acceptance cone will be. Provided the neutrons are incident perpendicular to the fibres' axis, the number of fired fibres will decrease for large recoil angles. An energy threshold, by means of a condition on the number of fired fibres, affects the efficiency of the detector, much in the same way as a pulse amplitude discrimination level does for a large scintillator.

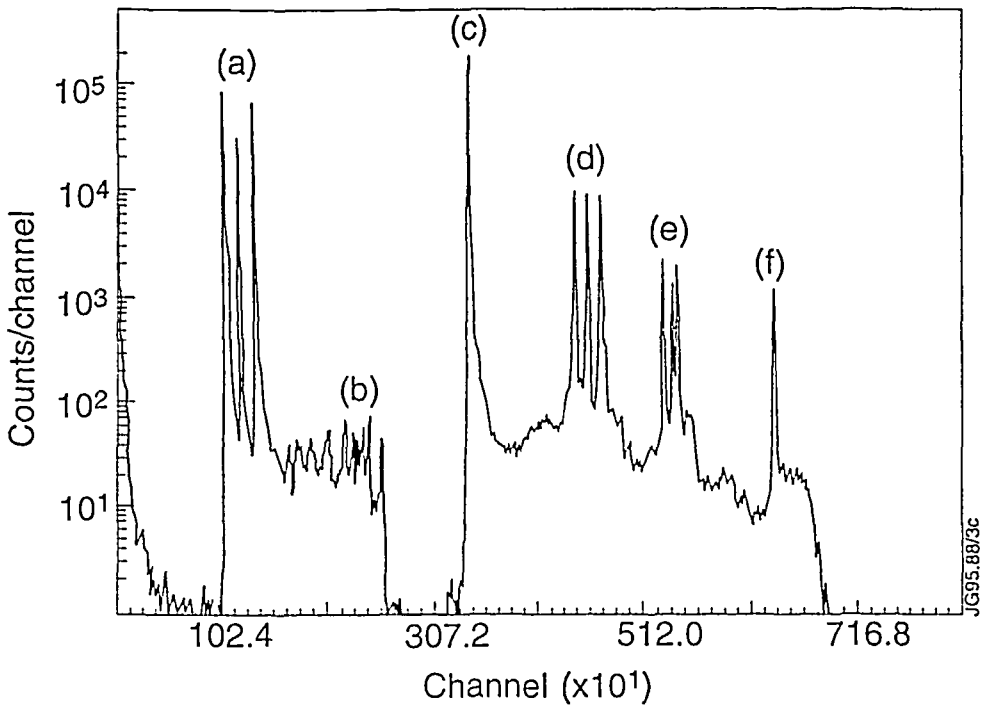

Fig. 16. Spectrum showing the number of fibres fired for a neutron source.

An experiment is designed to select only those signals, that satisfy well defined conditions on the number of fired fibres.

The PMT's are connected to CF4000 and from there to CF8000 in the same manner as described in section 4.1. The multiplicity output M on CF8000 is connected to two different signal chains using a T-connector. One leads to an amplifier which is used to amplify and shape the signal. The output from the amplifier is fed into a Single Channel Analyzer (SCA), which is used to create the desired amplitude window. Setting an amplitude window at the SCA is equivalent to setting a condition on the number of fired fibres. When a signal of the right amplitude appears at the input, the SCA will deliver a standard signal at its output, which is fed into the ADC gate input. The other signal is fed into an amplifier, shaped and delayed to match the timing of the gate pulse. In response to a signal within a set amplitude window, the SCA delivers a gate pulse to the ADC, which accepts the signal. The resulting spectrum will only show signals within the window. A schematic view of the electronics is seen in Fig. 17..

Obtained spectra show signals only within the set amplitude window as expected. However, some signals are excluded, despite having the right amplitude. It seems like the SCA does not provide gate pulses for all the signals of the right amplitude. This may possibly be due to cable reflections in the crude experimental set-up.

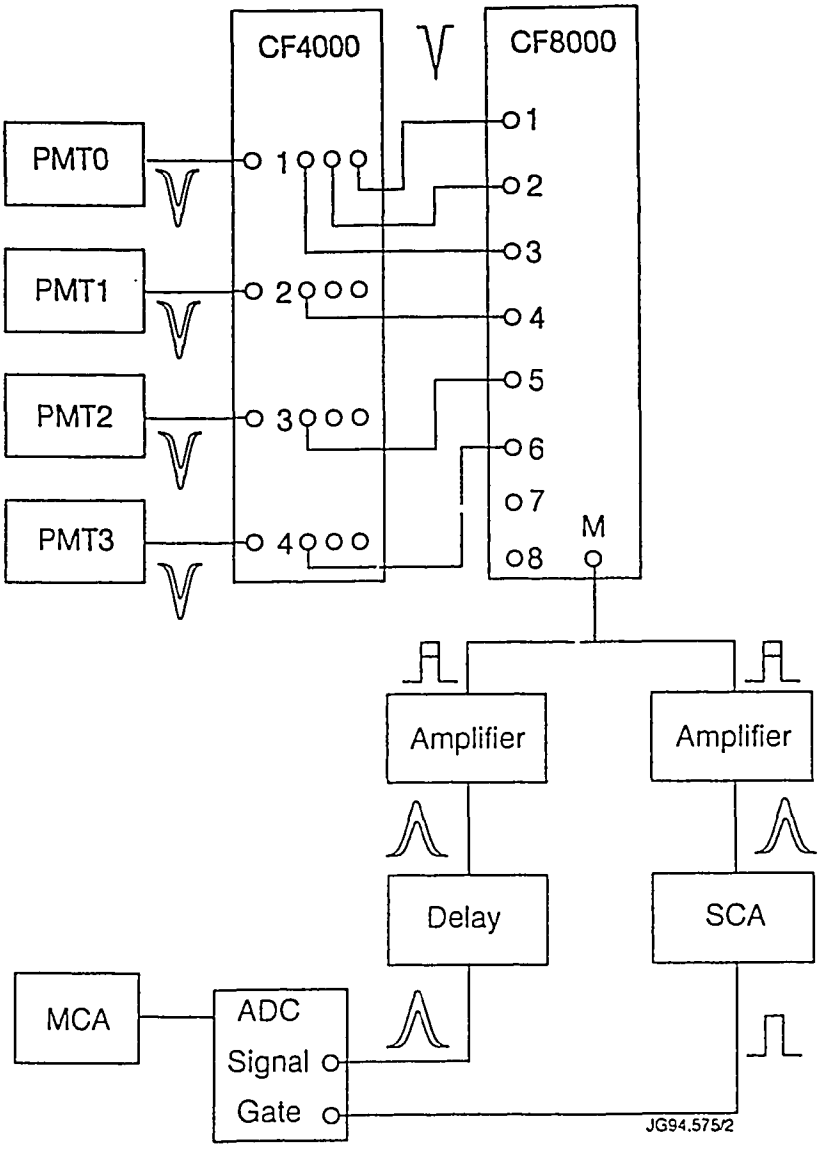

Fig. 17. The electronics set-up to select an energy window

4.3 Pulse height measurements

4.3.1 Adjustment of the PMT's supply voltages

In order to give the PM tubes a similar gain, a calibration procedure is performed. The procedure is based on measuring the true count-rate from a γ-source for the PMT1-3 at different supply voltages.

The tube of interest is connected to one of the channels on the CF4000. The same channel and the same discrimination level are used for all PMT's. The standard signals from the CF4000 are readily counted using an Ortec 874 quad counter/timer.

The number of counts are recorded during 60 seconds with and without the detector exposed to the ^{60}Co γ-source. The number of background counts is subtracted from the number of counts obtained with the source.

For all PM tubes except one, the number of true counts increases with supply voltage. The odd one out shows a decrease in the number of true counts instead of an increase. At a lower voltage it seems to behave in a more predictable fashion. The tube is limited for use in a low voltage range. Another of the tubes shows a slow increase in the number of true counts and this tube is used in a higher voltage range. The tubes 1-3 are found to have a similar number of true counts for the voltages in Table 2. The fraction of background counts is less than 22% for any PMT with these settings. The PMT0 voltage is set, so that it would give about three times the count-rate compared to any of the other tubes.

Table 2. The PMT supply voltages.

PMT	Supply voltage (kV)
0	-2.2
1	-1.89
2	-2.19
3	-2.4

4.3.2 Pulse height spectra

An important part of the experiments is the measurements of pulse heights, when the detector is irradiated with neutrons and γ, respectively. A first simple test is carried out using an oscilloscope directly connected to one PMT. Pictures of the response from PMT1 for background, γ and neutrons can be found in Fig. 18 a, b, c. The amplitude of the signals is estimated on the oscilloscope screen, with the result for different sources shown in Table 3.

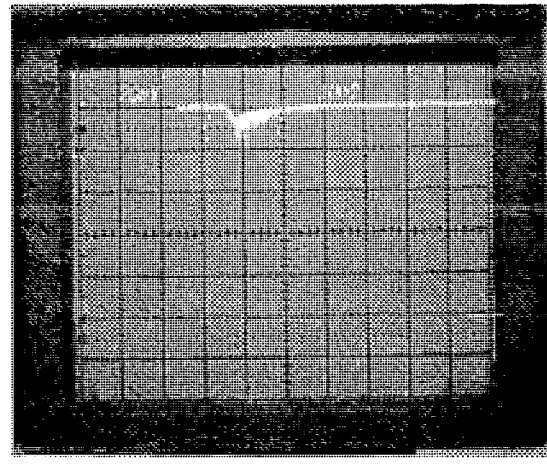

(a) X= 10 ns/div, Y= 20 mV/div

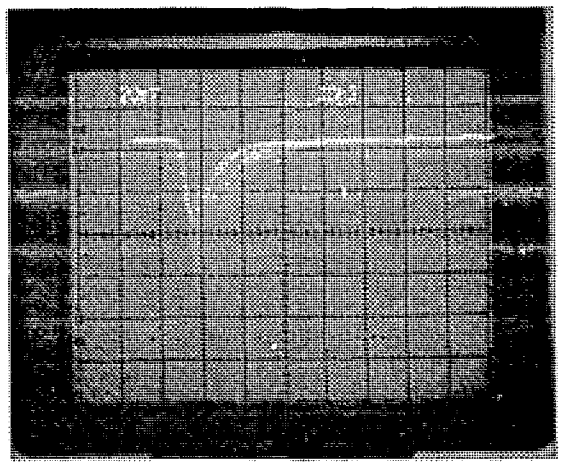

(b) X= 10 ns/div, Y= 20 mV/div

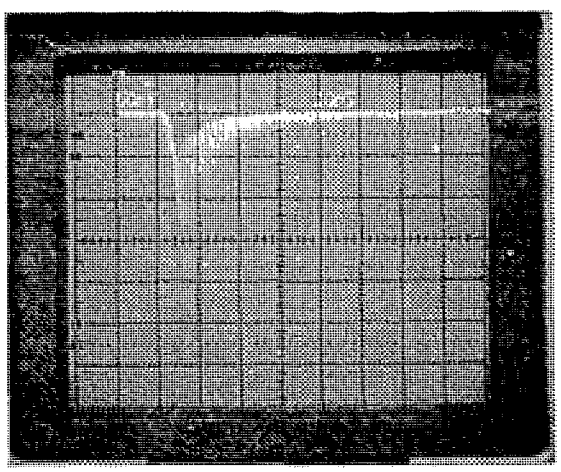

(c) X= 10 ns/div, Y= 50 mV/div

Fig. 18 a, b, c. Pictures of the oscilloscope screen showing the response from PMT1 for: a. background, b. ^{60}Co γ, and c. neutrons.

Table 3. Estimations of the maximum signal amplitude from background (B), γ (S_γ) and neutron induced events (S_n).

PMT	Background (mV)	^{60}Co γ (mV)	AmBe neutrons (mV)	S_n / S_γ / B
0	40	150	600	15 / 3.8 / 1
1	20	50	350	17 / 2.5 / 1
2	25	60	400	16 / 2.4 / 1
3	30	60	350	12 / 2.0 / 1

Measurements of pulse height spectra for γ and neutron radiation are performed. The PMT to be measured is connected to an Ortec 572 amplifier. After amplification and shaping the signal is fed into an Ortec 673 spectroscopy amplifier. The output of the spectroscopy amplifier is connected to the ADC input, and recorded by the MCA. The electronic set-up is shown in Fig. 19.

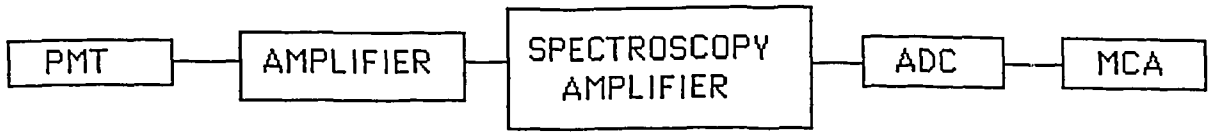

Fig. 19. A schematic view of the electronic set-up for pulse height measurements.

Pulse height spectra of events induced by electronic noise, radiation background, γ and neutron sources are recorded. The responses of PMT0 and PMT1 are found in Figs. 20 and 21. The figures are overlaid and show, from left to right, the response for: amplifier noise, background, ^{137}Cs γ, ^{60}Co γ and neutrons. These graphs have the number of counts per channel in a logarithmic scale on the vertical axis, and the signal amplitude in channels on the horizontal axis.

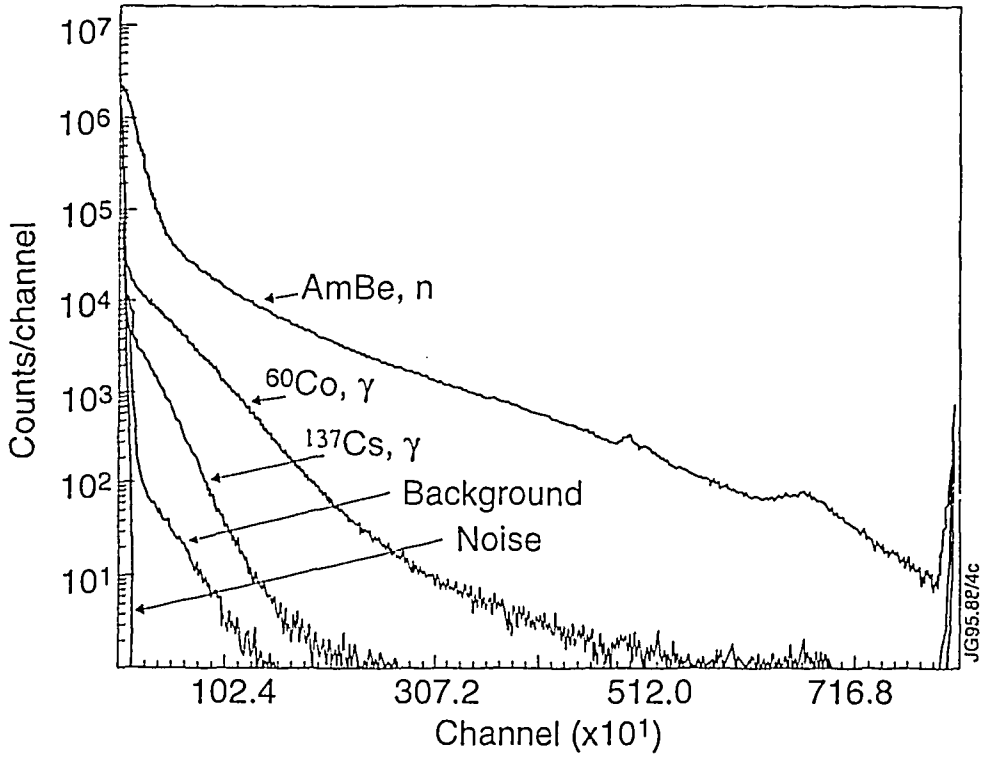

Fig. 20. Pulse height spectra from PMT0 for electronic noise, radiation background, γ and neutron sources.

These spectra show an exponential decrease of the number of counts with increasing pulse height. At low and high amplitudes the response differs from this behaviour. At very low amplitudes noise from the amplifiers dominate the spectra. At high amplitudes for each graph, there is a tail digressing from the exponential behaviour.
Comparing the response for γ and neutrons, it is seen that the neutron response reaches further up the amplitude scale than does the γ response. The recoil protons have shorter path lengths than Compton electrons and they can possess a lot more energy to deposit. The difference in amplitude range between γ and neutrons suggests the feasibility to discriminate against γ using pulse amplitude discrimination, although a quantitative ratio is not applicable. The optimum discrimination level can instead be determined for greatest neutron detection efficiency, under the constraint of a minimum fraction of interfering γ counts.

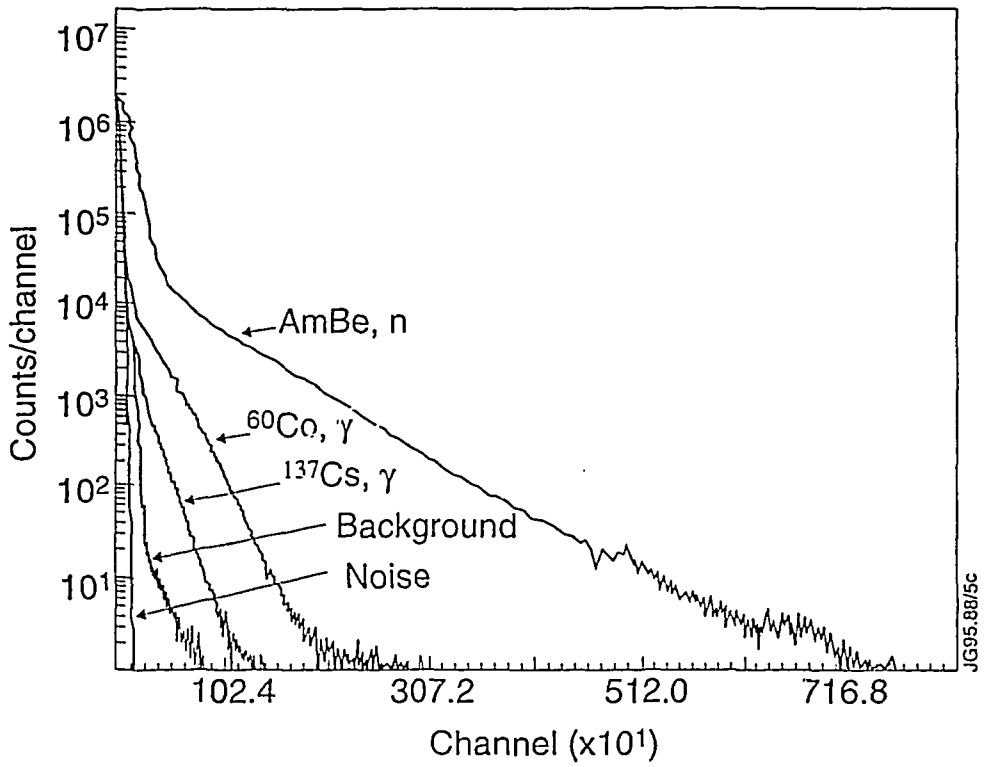

Fig. 21. Pulse height spectra from PMT1 for electronic noise, radiation background, γ and neutron sources.

Ideally the response for γ should resemble the Compton continuum, see Fig. 2. The rectangular recoil proton spectrum for neutrons, see Fig. 3, is not even ideally the response for a scintillator irradiated with neutrons from a AmBe source. This is due to the broad neutron energy spectrum from the source and the nonlinearity of the scintillator response to recoil protons. Further, different factors such as edge effects, light attenuation and the finite detector resolution distort the response. The possibility of particles escaping the fibres causes an edge effect, which shifts events from higher amplitudes to lower ones. Events close to the PMT's benefit from the light trapped in the cladding of the fibre. The "clad" light is strongly attenuated as it travels along the fibre. For events occurring further from the PMT's than a few cm, the "clad" light has been reduced to a negligible level and only the "core" light remains. Light attenuation affects the response much in the same way as edge effects.

Electrons have an approximately constant differential energy loss, see Fig. 4, and would therefore give the same light output for each penetrated fibre independent of their energy. PMT1 is connected to every third layer and Compton electrons with longer track lengths will add up their response, causing the amplitude to be dependent on the track length. Therefore, the γ response of PMT1, as well as that of PMT0, for ^{60}Co (1.17 MeV and 1.33 MeV γ energies) reaches a higher amplitude than the response for ^{137}Cs (0.662 MeV).

5. Discussion and conclusions

A test detector has been designed and constructed to test some features of scintillating fibres. Pulse height spectra show that recoil protons give larger signals than recoil electrons. Pulse amplitude discrimination of γ events therefore seems feasible. The spectra showing the number of fibres fired are greatly affected by light attenuation and events occurring in fibres outside the holder, making interpretations difficult.

From the oscilloscope we can estimate a maximum signal amplitude S_n/S_γ ratio of 6 for PMT1-3, see Table 3. In this case the PMT's are connected to every third layer, which means that γ signals can add up by passing through several layers connected to the same tube. A detector using enough PMT's to resolve the track of an electron, would share the deposited energy by the number of fibres in the track. The recoil protons on the other hand penetrate few fibres. Therefore, the ratio of the pulse heights for γ and neutrons should increase, when increasing the number of fibres connected to different photo detectors. E.g. a change from 3 to 18 layers connected to different PMT's, with otherwise unchanged conditions, would increase the maximum S_n/S_γ ratio to a factor of 30-40. Further increase in the number of layers will not increase the ratio, because then the track length of the electron is exceeded by the total length of the layers and no summation will occur.

5.1 Future experiments and extensions of the work

To properly develop this concept into a useful detector there are several aspects that should be considered. The following experiments are suggested to be carried out in the future:

- The light attenuation in the fibres introduces problems as discussed earlier. This could be avoided through utilization of good neutron and γ collimation in the experiments.

- Test of the neutron and γ responses with different fibre sizes. Smaller fibres are expected to give better S_n/S_γ ratio than larger fibres, but this should be confirmed. Experiments should also confirm that increased efficiency, i.e. by adding more fibre layers to the detector, can be achieved with maintained ability to separate neutron and γ induced events.

- Monte-Carlo calculations should be employed to calculate the efficiency and the response to neutron and γ-radiation.

- Experiments should be performed with a multichannel PMT and a complete detector geometry, as the one described in Appendix 2. This could be used to test the response to neutron and γ radiation, the energy window and the ability to detect 14.1 MeV neutrons in a background of γ and low energy neutrons. The count-rate capability of the fibre detector should also be tested.

5.2 Future applications

A full scale detector of this type can be one alternative for a neutron flux detector for measurements of neutron fluxes in various experiments. An outline of a scintillating fibre system, interesting for use at the future ITER fusion tokamak experiment, is given in Appendix 2.

Another fusion experiment of interest is the planned W7-X Stellarator in Greifswald, Germany. If the decision to build this machine is taken, the fibre system could be used for flux measurements of 2.45 MeV neutrons.

Other applications using fibres include detectors in the field of high energy physics, for example particle detectors at CERN. Spectrometers for measuring the energy of different particles, tracking detectors recording the path of the particle and detectors being able to record multiple hits simultaneously.

In general, scintillating fibre systems for detecting particles will be of great interest in the future. Developments of better scintillating materials, multichannel PM tubes and new improved APD's (Avalanche Photo Diodes) boost one of the oldest techniques for radiation detection to new heights. New fast electronics which is capable of handling large amounts of data rapidly, open up possibilities of using large systems and complex geometries of scintillating optical fibres.

Acknowledgements

This diploma thesis project has been carried out during the summer of 1994 at the Department of Reactor Physics, Chalmers University of Technology. I am grateful for all help I received during this work. Especially I would like to thank Dr. Thomas Elevant, my supervisor who initiated the study of scintillating fibres for use in neutron detectors, and Ph.D. student Per Lindén, who has made valuable suggestions regarding this work.

References

1. W R Binns, M H Israel and J Klarmann. "Scintillator-Fiber Charged-Particle Track-Imaging Detector", Nucl. Instr. and Meth. 216(1983)475.

2. A Konaka, et al., "Plastic Scintillating Fibers for Track Detection", Nucl. Instr. and Meth. A256(1987)70.

3. F G Hartjes and R Wigmans, "Scintillating Plastic Fibres for Hadron Calorimetry", Nucl. Instr. and Meth. A277(1989)379.

4. H Burmeister, P Sonderegger, J M Gago, A Maio, M Pimenta, D Perrin and J C Thevenin, "Electromagnetic Calorimetry using Scintillating Plastic Fibers", Nucl. Instr. and Meth. 225(1984)530.

5. C Angelini, et al., "WA84 Experiment: A Beuty Search with a Scintillating-Fibre Microvertex Detector", Nucl. Instr. and Meth. A289(1990)342.

6. C Fisher, "From Bubble Chambers to Scintillating Fibres: High Resolution Particle Tracking for Microvertex Detection", Nucl. Instr. and Meth. A263(1988)159.

7. Y Yariv, R C Byrd, A Gavron and W C Sailor, "Simulations of Neutron Response and Background Rejection for a Scintillating-fiber Detector", Nucl. Instr. and Meth. A292(1990)351.

8. Magnus Hoek, "Development and Use of Neutron Scintillation Systems for Fusion Plasma Diagnostics", Report CTH-RF-93. Chalmers University of Technology, Goteborg (1992).

9. J B Birks, "The Theory and Practice of Scintillation Counting", Pergamon Press, Oxford (1964).

10. G F Knoll, "Radiation Detection and Measurement", John Wiley & Sons. (1989).

11. T O White, "Scintillating Fibres", Nucl. Instr. and Meth. A273(1988)820.

12. C M Hawkes, M Kuhlen, B Milliken, R Stroynowski, E Wicklund, T Shimizu and O Shinji, "Decay Time and Light Yield Measurements for Plastic Scintillating Fibers", Nucl. Instr. and Meth. A292(1990)329.

13. R Madey, F M Waterman, A R Baldwin, J N Knudson, J D Carlson and J Rapaport, "The Response of NE-228A, NE228, NE224 and NE102 Scintillators to Protons from 2.43 to 19.55 MeV", Nucl. Instr. and Meth. 151(1978)445.

14. C N Chou, Phys. Rev. 87(1952)904.

15. R L Craun and D L Smith, "Analysis of Response Data for Several Organic Scintillators", Nucl. Instr. and Meth. 80(1970)239.

16. W W Lindstrom and B D Anderson, Nucl. Instr. and Meth. 98(1972)413.

Appendix 1. The properties of BCF12 scintillating fibres

The fibres used in this work are BCF12 blue scintillating fibres, manufactured by Bicron corporation. Some data on the fibers are presented in Table 4.

Table 4. Properties of the BCF12 scintillating fibres. If not else stated, the values apply to the core of the fibres. These values come from the manufacturer's data sheet.

Emission peak	435 nm
Decay time	3.2 ns
Attenuation length	2.2 m
Light yield	approx. 8000 photons/MeV
Core index	1.60
Cladding index	1.49
Density	1.05 g/cm^3
Cladding thickness	4% of fibre width
H/C ratio	0.994
Trapping efficiency	4.4%

The core of the fibres consists of a solid solution of a fluorescent organic scintillator dissolved in a polystyrene plastic. The cladding is made of PMMA (polymethylmethaacrylate, $C_5H_8O_2$) with a density of 1.2 g/cm^3 and a thickness of 4% of the fibre width. EMA (extra mural absorber) coating the outer surface of the fibre prevents cross-talk between adjacent fibres. The EMA coating is typically 10 to 15 μm thick.

Appendix 2. A brief topic report concerning the proposed scintillating fibre neutron flux detector for ITER.

ITER Diagnostics, Neutron working group

Scintillating Fibre Neutron Flux Detector

T Elevant with contributions from J Karlsson, *Dep. of Reactor Physics, Chalmers University of Technology, Gothenburg, Sweden.*

INTRODUCTION

A detector based on scintillating fibres is proposed to be used in the neutron profile camera. The aim is to measure collimated neutron fluxes $\phi n = 10^5$-10^8 n/(cm^{2}s) with an accuracy of 5%, time resolution of 100 - 0.1 ms and an energy range from 10-18 MeV.

TECHNIQUE

Alternate orthogonal planes made of thin scintillating fibres are used to build a compact detector with a volume of a few cm^3. The fibre axes are oriented perpendicular to the incident neutron beam direction. The pattern of fibres fired provides a coarse measure of the neutron energy. Different specific light output from protons and electrons enables signals from neutron and gamma interactions to be separated by means of pulse amplitude discrimination of signals from individual fibres. Thus, the detector has a thin scintillator's ability to separate neutron from gamma events, still maintaining the efficiency of a thick detector. A collimator with only a few cm^2 cross-section area at the first wall is used. The fast response of the scintillating fibres enables useful count-rates of several MHz to be obtained. Results from neutron and gamma transport calculations for a similar neutron detector are given in Ref. [1].

PROPOSED DESIGN

Square shaped, 0.3 mm, scintillating fibres of 10 mm lengths are spliced to clear fibres and connected to a multi-channel PMT. Only the proton track length and its orientation are important but not its position. Therefore, two sides of the detector are divided into 80 modules. Each module consists of 4*6 fibre ends, which are connected to 24 PMT channels. This is repeated for an adjacent detector side, forming a 3D picture of the proton track by means of two 2D pictures. The 3840 fibres occupy 70% of the available cathode area of one PMT. Fig. 22 shows the outline of the detector system.

Signal electronics provide pulse amplitude discrimination of each of the 48 ch's. The resulting 48 bit digital word contains coarse information on the proton energy and recoil angle. A digital filter is applied to select events with neutron energies of 10-18 MeV.

IMPORTANT CONSIDERATIONS

The light output is essential for the performance of this detector. Considering scintillating-, trapping- and light conversion efficiencies, a 14 MeV recoil proton, traversing the first 0.3 mm fibre, generates approximately 40 photo-electrons. The specific energy loss increases for lower energies, giving an increased photon yield from successive completely penetrated fibres.

Tests have given signal amplitude ratios from neutron, gamma and background events equal to $S_n/S_\gamma/B$ = 10/2.5/1 for 0.2 mm square fibres. Glass capillaries can sustain very high doses [2], corresponding to 70 000 full power discharges of 10^3s duration in fluxes of 10^8 n/(cm^{2}s). Plastic fibres can sustain 100-500 discharges before suffering from radiation damages.

R&D WORK

Few attempts have been made to use scintillating optical fibres for detection of fast neutrons. Therefore some studies to examine different important issues are suggested:

- Monte-Carlo calculations of the efficiency and energy range of the detector.

- Tests of efficiency, maximum count-rates, radiation damages and neutron/gamma separation capabilities.

- Design, construction and test of a full scale prototype at a neutron generator and at JET.

REFERENCES

[1] Y Yariv et al. NIM A292 (1990)
[2] M Adinolfi et al. NIM A315 (1992)

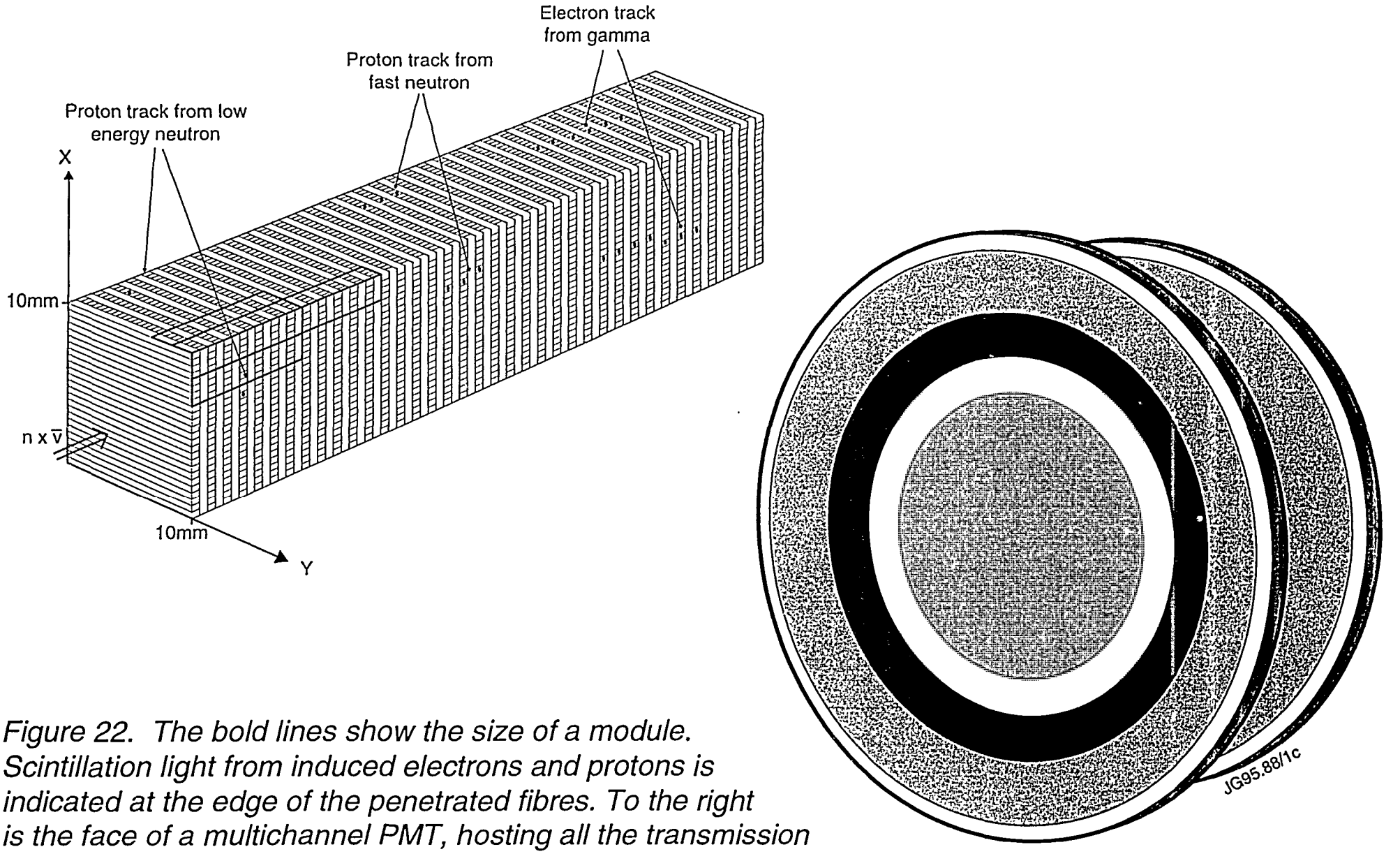

Figure 22. The bold lines show the size of a module. Scintillation light from induced electrons and protons is indicated at the edge of the penetrated fibres. To the right is the face of a multichannel PMT, hosting all the transmission fibres from the detector.